Influence of Fibrosis Amount and Patterns on Ventricular Arrythmogenesis and Pumping Efficacy: Computational Study

Abrha Abebe Tekle
Kumoh National Institute of Technology
Ki Moo Lim (kmlim@kumoh.ac.kr)
Kumoh National Institute of Technology https://orcid.org/0000-0001-6729-8129

Research

Keywords: Fibrosis, arrhythmogenesis, phase singularity, fibrosis entropy, stroke volume, computational study

Posted Date: March 26th, 2020

DOI: https://doi.org/10.21203/rs.3.rs-19126/v1

Influence of Fibrosis Amount and Patterns on Ventricular Arrythmogenesis and Pumping Efficacy: Computational Study

Abrha Abebe Tekle[1] and Ki Moo Lim[2]*

[1]*Department of IT Convergence Engineering, Kumoh National Institute of Technology, Gumi, Republic of Korea*

[1]*E-mail: abe.habesha@gmail.com*

[2*]*Department of IT Convergence Engineering, Kumoh National Institute of Technology, Gumi, Republic of Korea*

[*2]*E-mail: kmlim@kumoh.ac.kr*

Running title: Myocardial Fibrosis and Cardiac Pumping Efficacy

[*]**Corresponding author:**

[*]Professor Ki Moo Lim, PhD

[*]*Department of IT Convergence Engineering, Kumoh National Institute of Technology, 61 Daehak-ro, Gumi, Gyeongbuk 39177, Republic of Korea*

Tel.: +82 54-478-7785

Fax: +82 54-478-7859

[*]E-mail: kmlim@kumoh.ac.kr

Abstract

Background and aims: Clinical and computational studies have reported that spatial fibrosis pattern and fibrosis amount play a significant role in ventricular arrhythmogenicity. Nonetheless, the underlying mechanisms of arrhythmogenicity of fibrosis are not known accurately. In addition, we believe that the effect of different fibrosis types and fibrosis amount on the cardiac mechanical performance requires a further investigation. Therefore, this study investigated the effect of spatial distribution of fibrosis and fibrosis amount on the electrical and mechanical performance of the left ventricle (LV).

Methods: We employed a human ventricular model that simulates both the electrophysiological and the mechanical contraction characteristics of the ventricle. The electrophysiological conduction model mimics the exchange of ions through the plasma membrane of myocardial cells whereas the mechanical contraction model simulates the mechanical cardiac response. Seventy-five fibrosis distributions comprising diffuse, patchy, and compact fibrosis types that contain 10%–50% fibrosis amount were generated to cover a wide range of fibrosis cases. The spatial fibrosis distribution in the human ventricular model was quantified using fibrosis entropy (FE) metric. Then, electrophysiological simulations under reentry conditions induced using the S1-S2 protocol were conducted to investigate the correlation between different patterns of fibrosis and ventricular arrhythmogenicity. Finally, we compared the mechanical response by conducting mechanical simulations to examine the influence of the fibrosis amount and spatial distribution of fibrosis on the pumping efficacy of the LV by extracting the calcium information from the electrophysiological simulation.

Results: We observed that the spatial patchy fibrosis distribution was more chaotic (higher mean FE) than those of the compact and diffuse types. The electrical simulation results revealed that the ventricular arrhythmogenicity of diffuse fibrosis depends on the fibrosis amount and marginally on the spatial distribution of fibrosis. Meanwhile, the ventricular arrhythmogenicity of the compact and patchy fibrosis types is reliant on the spatial distribution of fibrosis than on the fibrosis amount. The average number of phase singularities in the electrical simulations with compact fibrosis was higher than those with patchy and diffuse fibrosis. As a result, compact fibrosis resulted a lower stroke volume (SV) of the LV, whereas the diffuse fibrosis resulted in a higher SV of the LV. The

reduction in the stroke volume (SV) of the LV was linearly correlated to the electrical instabilities induced by the fibrosis amount and spatial distribution of fibrosis.

Conclusion: The increase in the amount of diffuse, patchy and compact fibrosis in the myocardium increased the electrical instability and likely decreased the pumping efficacy of LV. Moreover, the effect fibrosis pattern on ventricular arrhythmogenesis was more significant in compact and patchy fibrosis types than in diffuse fibrosis.

Key words: Fibrosis, arrhythmogenesis, phase singularity, fibrosis entropy, stroke volume, computational study

Background

A cardiac extracellular matrix (ECM) is a sophisticated network of structural components. It constitutes up to 6% of the myocardium wall. The ECM consists of non-excitable cells called fibroblasts. Fibroblasts produce components that constitute the ECM, e.g., collagen [1]. The ECM provides strength and support to myocytes. In addition, it maintains the myocardial structure and provides a three-dimensional (3D) scaffold [1, 2]. Thus, it plays a significant role in determining the mechanical properties of the heart and electrical impulse propagation.

Owing to aging or heart diseases, the amount of ECM in the myocardium increases substantially and instigates cardiac tissue remodeling. This is because of the proliferation of activated fibroblasts followed by an excessive deposition of collagens in the ECM, which is referred to as fibrosis [3, 4]. The percentage of connective tissue in the heart increases by up to 40% because of fibrosis [5]. Fibrosis occurs mostly to produce replacement for dead myocytes, to preserve the myocardial structure after myocardial infarction. Hence, fibrosis affects the

injured areas as well as the myocytes in the vicinity. Other conditions that cause replacement fibrosis are hypertrophic cardiomyopathy, sarcoidosis, myocarditis, chronic renal insufficiency, and toxic cardiomyopathies [6]. Fibrosis may occur as a reaction to different cardiomyopathies as those associated with hypertension and diabetes.

Studies have demonstrated that atrial and ventricular arrhythmogenesis increase linearly with an increase in fibrotic tissue [7-11]. Nonetheless, the underlying mechanisms of arrhythmogenicity of fibrosis are not known accurately. However, because fibrotic tissue by itself does not become involved in electrical activation, it is considered that the conduction delay caused by fibrosis plays a significant role. In areas with an increased amount of fibrosis are isolated from each other by collagen. Thus, the electrical propagation is compelled to adopt a discontinuous and zig-zag pattern through the tissue, from one myocyte strand to another [12, 13]. The circuitous conduction pathway reduces the conduction velocity. In addition, fibrosis causes unidirectional conduction block owing to the source–sink mismatch between the myocyte strands and neighboring normally-coupled tissue [14, 15]. The effect of fibrosis in promoting conduction delay and unidirectional blocking generates an environment suitable for reentry initiation, thereby escalating cardiac arrhythmias to heart failure. Moreover, clinical studies indicate that the fibrosis amount per se does not promote cardiac arrhythmia. The spatial distribution of fibrosis also exacerbates the arrhythmogenicity [5, 16]. In general, fibrosis may occur in different distinct forms: diffuse, compact, interstitial, and patchy [17]. These forms exhibit different arrhythmogenesis profiles depending on how they affect conduction delay and unidirectional blocking.

Several computational studies have been conducted to better understand the mechanisms of fibrosis arrhythmogenicity. Petrov [18] demonstrated that the texture of fibrotic tissue may cause anisotropic propagation and defragmentation of scroll wave, and alter the rotation of scroll waves. Similarly, Turner et al employed a human ventricular tissue model and demonstrated that fibrotic tissue with a string-like form causes defragmentation of electrogram [19]. By using different ion models, other studies' have also revealed that diffuse fibrosis increases the vulnerability of tissue to reentry [20-24]. Kazbanov et al. [25] studied the effect of fibrosis amount and degree of fibrosis heterogeneity. They observed that the onset of arrhythmias is more likely increased when the size of fibrosis and degree of fibrosis heterogeneity is larger.

Although the previous studies revealed that fibrosis tissue could result in increased vulnerability to reentry, none of them investigated or compared the effect of different fibrosis types and fibrosis amount on the perpetuation of arrhythmia and on the cardiac mechanical performance, which is the main function of the heart.

In this study, we investigated the influence of the fibrosis amount and spatial distribution of fibrosis on ventricular arrhythmogenesis and the pumping performance of ventricles, using an electromechanical model. To achieve this, 75 fibrosis distributions consisting of various forms of fibrosis patterns including diffuse, compact, and patchy were generated. Fibrosis density of up to 50% was employed in this study. We calculated the fibrosis entropy (FE) to quantify and better understand the level of disorganization of the fibrosis distribution. We performed electrical simulations under reentry conditions and examined how the various fibrosis distributions and fibrosis densities contribute to the perpetuation

of arrhythmia. In addition, we investigated how electrical instabilities induced by fibrosis affect the mechanical performance of the left ventricle.

Methods

Electrophysiological and mechanical model

To investigate the arrhythmogenesis of fibrosis, we employed a ventricular excitation–contraction (E–C) coupling model that comprises the electrophysiological and mechanical properties. The electrophysiological conduction model mimics the exchange of ions through the plasma membrane of myocardial cells (Fig. 1). The ion model of Ten Tusscher et al. was used to simulate the ventricular cardiomyocyte behavior [26]. The action potential propagation in myocardial tissue was imparted using the following partial differential equation:

$$\nabla \cdot \tilde{\sigma} \nabla V_m = \beta I_m \tag{1}$$

$$I_m = C_m \frac{\partial V_m}{\partial t} + I_{ion}(V_m, v) - I_{trans} \tag{2}$$

$\tilde{\sigma}$ is the intracellular conductivity tensor, β is surface – volume ratio of cardiac cells, I_{trans} is current density of the transmembrane stimulus, C_m is membrane capacitance per unit area, V_m is membrane potential, and I_{ion} is current density of the ionics current, which depends on the transmembrane potential and other state variables represented by v. I_{ion} is the sum of all transmembrane ionic currents given by the following equation.

$$I_{ion} = I_{Na} + I_{K1} + I_{to} + I_{Kr} + I_{Ks} + I_{CaL} + I_{NaCa} + I_{NaK} + I_{pCa} + I_{pK} + I_{bCa} + I_{bNa} \tag{3}$$

I_{Na} is the fast Na^+ current, I_{K1} is the inward rectifier K^+ current, I_{to} is the transient outward current, I_{Kr} is the rapid delayed rectifier current, I_{Ks} is the slow delayed rectifier current, I_{CaL} is the L-type Ca^{2+} current, I_{NaCa} is the Na^+/Ca^{2+} exchanger current, I_{NaK} is the Na^+/K^+ pump current, I_{pCa} and I_{pK} are the plateau Ca^{2+} and K^+ currents, respectively, I_{bCa} and I_{bK} are the respective background Ca^{2+} and K^+ currents. The equations for these ionic currents are specified in the membrane current; please refer to Ten Tusscher et al. [26] for details on each equation. Finite tetrahedral linear elements were generated by using HyperMesh software (214,319 nodes and 1,061,379 elements).

The electrophysiology mechanism and conduction properties were modified to represent the fibrotic regions. The non-fibrotic action potential model provided by Ten Tusscher et al [26] was modified as follows to represent the regional electrophysiological owing to fibrotic remodeling: 50% reduction in I_{K1}; 50% reduction in I_{CaL}; and 40% reduction in I_{Na} [27, 28]. Furthermore, the conductivity values in the fibrotic regions were reduced by 30% to simulate the conduction delay caused by fibrosis [29, 30].

E–C coupling was implemented by applying the calcium transient data extracted from the electrophysiological simulation to the mechanical simulations to induce contraction of the myofilaments and generate tension through Ca^{2+}-induced Ca^{2+}-release (CICR) current. The mechanical cross-bridge cycling model provided by Rice et al. was applied to simulate mechanical cardiac response [31]. The calcium dynamics to generate the calcium transients can be represented using the following equations:

$$\frac{dCa_{itotal}}{dt} = -\frac{I_{Ca,L}+I_{b,Ca}+I_{p,Ca}-2I_{Na,Ca}}{2V_CF} + I_{leak} - I_{up} + I_{rel} \quad (4)$$

$$\frac{dCa_{srtotal}}{dt} = \frac{V_c}{V_{SR}}(-I_{leak} + I_{up} - I_{rel}) \quad (5)$$

where Ca_{itotal} is the total amount of calcium in the cytoplasm and $Ca_{srtotal}$ is the total amount of calcium in the sarcoplasmic reticulum (SR). I_{rel} is the calcium current released from the junctional SR (JSR), and I_{leak} is the leakage calcium current of the JSR. I_{up} is the absorbed calcium current in the network SR (NSR), and I_{xfer} is the diffusible calcium current between the dyadic subspace and bulk cytoplasm.

Mathematical description of mechanical contraction of cardiac tissue is based on continuum mechanics [32, 33], with myocardium assumed to be hyper-elastic, nearly incompressible material, the passive mechanical properties of which were defined by an exponential strain function [33].

$$W = \frac{\mathrm{C}}{2}(e^{Q} - 1) \quad (6)$$

$$\mathrm{Q} = b_1 E_{ff}^2 + b_2(E_{rr}^2 + E_{cc}^2 + 2E_{rc}^2) + 2b_3\left(E_{fr}^2 + E_{fc}^2\right) \quad (7)$$

where W is a strain energy function, the Langian Green's strains E_{ij} are referred to the local fiber coordinate system. C is 2kPa, b_f is 8, b_t is 2, b_{fs} is 4. The laminar sheet and fiber orientation information determined the orthotropic electrical conductivity and passive mechanical properties of the myocardium. A finite element mesh consisting of 462 nodes and 230 Hermite elements were used. Cross-bridge dynamics model [31] represented the generation of active tension at the level of single myocyte.

To simulate hemodynamic responses, which are the interactions between the blood and ventricles, the finite element electromechanical model of the human ventricle was coupled with a circulatory model using the coupling method of

Gurev et al. [34] A schematic diagram of the integrated model is illustrated in Fig. 1.

Fibrosis distribution

In this study, 25 ventricular models with diffuse fibrosis distributions, 25 with patchy fibrosis distributions, and 25 with compact fibrosis distributions, i.e., a total of 75 ventricular models were employed. The fibrosis amount in the ventricular models is 10%, 20%, 30%, 40%, and 50%. The diffuse fibrosis patterns were generated by randomly assigning fibrosis information to the nodes in the ventricular model. The areas of patchy fibrosis were obtained manually such that the fibrosis regions isolate cardiomyocytes over extended distances. Compact fibrosis regions, which are characterized by large dense areas of fibrosis tissue lacking cardiac myocytes, were generated by forming various groups of fibrosis regions in different locations of the ventricular mesh.

Quantification of spatial distribution of fibrosis

To better understand the spatial fibrosis distribution in each ventricular model, we calculated the local FE of each element. The local FE of the i^{th} element was calculated to indicate the level of chaos within the element and its neighboring elements. It is expressed using Shannon entropy equation (10) [35].

$$FE = \sum_{i=1}^{N} \frac{-P_i ln(P_i)}{N} \quad (8)$$

N denotes the i^{th} element and all its neighboring elements. F is the total number of fibrotic elements that are neighbors of the i^{th} element. P_i is the ratio of the number of elements that are different from the i^{th} element to the total number of neighboring elements.

Simulation protocol

To assess the effect of the fibrosis amount and spatial distribution, a series of 3D electromechanical simulations were conducted under reentry condition. In the electrical simulation, reentry was initiated using the standard S1-S2 protocol. First, three S1 electrical stimuli were applied at the apex of the ventricle with 600 ms BCL. This produced a planer wavefront that propagated toward the top of the ventricle. When the wavefront of the last S1 stimulus reached half of the ventricle, the left side of the ventricle was artificially reset to resting membrane potential. This caused the wavefront to propagate toward the artificially reset region, producing a spiral wave. For each fibrosis distribution, we conducted electrical simulations to investigate the range of conduction velocity at which the reentrant wave sustained and failed to sustain. After we determined the optimum conduction velocity that sustained the reentrant wave under all fibrosis density and distributions, we quantified the electrical instability caused by fibrosis. To achieve this, we calculated the phase singularities (PSs) from the results of the electrical simulations, using the Iyer and Grey method [36].

After finishing our investigation of the arrhythmogenesis of fibrosis, we studied the effect of the electrical instability induced by fibrosis on the pumping performance of the LV. To achieve this, we performed a mechanical simulation of each fibrosis distribution by extracting calcium transient information from its respective 3D electrophysiological simulation to mimic the cardiac E-C coupling. We compared the SV, which is amount of blood pumped out of the left ventricle during its contraction, under all the fibrosis distributions.

Results

Fibrosis distributions

Fig. 2 shows the generated diffuse, patchy and compact fibrosis types with fibrosis amount 0% to 50%. In diffuse fibrosis distributions, small fibrotic tissue is interspersed randomly among myocytes in all parts of the ventricle (Fig. 2A). In compact fibrosis, fibrosis tissue exists as a large dense area of fibrosis (Fig. 2C). These dense fibrotic regions mimic large scars in the myocardium caused by myocardial infarction or other chronic diseases. The large scars are devoid of cardiac myocytes. Patchy fibrosis distributions exhibit a string-like texture and isolates myocytes over long distances (Fig. 2B). These fibrosis regions do not entirely consist of fibrotic nodes. Some non–fibrotic nodes are also embedded. Thereby, normal myocytes are loosely interconnected to each other.

Quantification of fibrosis spatial distributions

The spatial distribution of fibrosis patterns was quantified by calculating the local FE of each node that constituted the ventricular model. Fig. 3 illustrates the mean FE (MFE) of diffuse, compact, and patchy fibrosis patterns with fibrosis amount 10%–50%. The computation of MFE for each fibrosis type involved the following procedures. First, the local FE of all the nodes in a ventricle was computed according to the spatial fibrosis distribution in each ventricular model. Second, the mean FE of all the nodes was calculated. Because there are five different distributions in each fibrosis type that have equal fibrosis amounts, the average FE of these five distributions was then calculated. The MFE increased in all the fibrosis forms as the fibrosis amount increased from 10% to 50%. It is evident that the MFE of the patchy patterns was larger than that of the compact and diffuse patterns for all the fibrosis amounts. This demonstrates that the fibrosis distribution in the patchy fibrosis pattern is more chaotic than in compact and diffuse. When the fibrosis amount was 10%–40%, the compact fibrosis

patterns exhibited higher MFE than the diffuse ones. However, at 50% of fibrosis amount, the diffuse patterns exhibited larger MFE than the compact ones.

Fibrosis arrhythmogenicity

We performed electrical simulations under reentry conditions to assess the influence of fibrosis on the electrical instability of ventricles. We investigated the length of conduction delay imposed by fibrosis in each fibrosis distribution, by applying conduction velocities (CVs) from 53 cm/s to 100 cm/s and examining whether reentry sustained or not. Electrical simulations involving ventricular models with diffuse fibrosis patterns revealed that the CV required to sustain the induced reentrant wave increased as the fibrosis amount increased from 10% to 50% (Fig. 4A). The conduction delay as a result of fibrosis was strongly correlated to the fibrosis amount in the myocardium. As mentioned in the previous section, diffuse fibrosis exhibits lower MFE than patchy and compact (Fig. 3). This implicates that ventricular models that contain an equal amount of diffuse fibrosis exhibit similar fibrosis textures. Thereby, different fibrosis distributions with equal fibrosis amount exhibited similar arrhythmogenesis. For example, 20% of the diffuse fibrosis distributions exhibited equal arrhythmogenesis. In addition, 30% of the diffuse fibrosis distributions exhibited similar arrhythmogenesis. In the remaining distributions, which had equal fibrosis amounts, the variation in arrhythmogenicity was marginal.

In electrophysiological simulations conducted under the patchy fibrosis type, the CV required to sustain the reentrant wave increased inconsistently with the fibrosis amount. Arrhythmogenesis was more reliant on the spatial distribution of fibrosis than on the fibrosis amount (Fig. 4B). This is apparent in some of the simulation results. For example, the conduction delay induced owing to fibrosis in two simulations with 10% fibrosis was longer than that in four simulations with 20% fibrosis and in two simulations with 30% fibrosis. Moreover, we detected

that two cases of 30% fibrosis induced longer conduction delay than two cases of 40% and two of 50% fibrosis. It is also evident that 50% fibrosis imposed conduction delay equal to that by 10% fibrosis. Furthermore, simulations under equal fibrosis amount with different distributions displayed different arrhythmogenesis. Because a patchy fibrosis distribution exhibits a higher disorganization (higher MFE) (Fig. 3), arrhythmogenesis of patchy fibrosis depends more on the spatial distribution than on the amount of fibrosis in the ventricular model.

In electrophysiological simulations conducted under compact fibrosis pattern, the CV required to sustain a reentry wave increased inconsistently with the fibrosis amount. It is also crucial to note that variation in the spatial distribution also conduction delay. Fig. 4C reveals that 10% and 20% fibrosis yielded identical conduction delay profile. The arrhythmogenicity in a case of 30% fibrosis was lower than that in all the cases of 20% fibrosis, and a case of 40% fibrosis exhibited arrhythmogenicity equal to the cases of 10% and 20% fibrosis. A few of the simulation results also revealed that 40% fibrosis tends to exhibit better arrhythmogenicity than 50% fibrosis. This is owing to the moderate disorganization in the distribution of compact fibrosis in the ventricular models.

Electrical instability owing to fibrosis

Phase singularity (PS) represents the core of a spiral wave or a rotor in ventricular fibrillation. We calculated the number of PSs to characterize the electrical instability induced by fibrosis. The average number of PSs during 8 s of simulation time was employed for analysis. Fig. 5A presents the average number of PSs caused by diffuse, patchy, and compact fibrosis types. For all the fibrosis amounts considered in this study, the average number of PSs in simulations applying compact fibrosis is higher than those applying patchy and diffuse fibrosis. Diffuse fibrosis caused a comparatively lower average number of PSs than those by patchy and compact fibrosis.

Mechanical Results

To examine the influence of the fibrosis type and fibrosis amount on the mechanical performance of ventricles, we conducted mechanical simulations by extracting calcium information from the results of electrophysiological simulation to mimic excitation–contraction coupling. We analyzed the SV when the mechanical response was relatively steady. Fig. 5B illustrates the average SV under diffuse, patchy, and compact fibrosis types. Overall, there was a significant reduction in the SV as the fibrosis amount in the ventricular model increased. Furthermore, the SV under diffuse fibrosis was higher than those under compact and patchy fibrosis. The SV under compact fibrosis was lower than those under patchy and diffuse fibrosis, except when the fibrosis amount was 40%. The reduction in the SV of the LV was linearly correlated to the electrical instabilities induced by the fibrosis amount and spatial distribution of fibrosis. The higher impact of compact fibrosis on electrical instability resulted in a lower LV-SV, whereas the lower electrical instability induced by diffuse fibrosis resulted in higher LV-SV. Patchy fibrosis marginally affected the electrical instability and also marginally reduced the mechanical performance of the LV.

Discussion

In this study, we investigated the effect of the fibrosis amount and spatial fibrosis distribution on electrical phenomena and the mechanical performance of ventricles under reentry conditions, by employing a human ventricular cardiomyocyte model. To our knowledge, this is the first systematic study carried out directly on the effect of the fibrosis amount and fibrosis patterns on the pumping capacity of the heart. The key observations of this study are as follows:

1. The CV required sustaining reentry increased consistently with an increase in diffuse fibrosis in the ventricular model. However, this correlation between CV and fibrosis amount is not consistent in the patchy and compact fibrosis types.
2. The average number of PSs detected in the electrophysiological simulations applying compact fibrosis was higher than those applying patchy and diffuse fibrosis. A lower average number of PSs was detected under diffuse fibrosis than under patchy and compact fibrosis.
3. The average LV-SV under compact fibrosis was lower than that under patchy and diffuse fibrosis.

Because fibrosis architecture varies across patients [37], we generated 75 different fibrosis distributions comprising diffuse, compact, and patchy fibrosis patterns based on Nguyen et al. [38]. In diffuse fibrosis, short collagen septa are interspersed among myocytes. Hence, we mimicked diffuse fibrosis by randomly distributing fibrosis information to the nodes that constitute the ventricular model. Compact fibrosis patterns were simulated as a large accumulation of fibrotic tissue devoid of healthy myocyte that resembles a large scar caused by myocardial infraction and other diseases. Patchy fibrosis patterns were represented as collagen fiber embedded among myocytes over a long distance. The maximum amount of fibrosis in a myocardial wall used in our study was 50%. This is based on a previous study's result, namely that the fibrosis amount in a chronically diseased heart may increase by up to 43% [5]. We developed a 3D map of the local FE of each element in the ventricular model for a better understanding the level of disorganization of the fibrosis spatial patterns. Our results demonstrated that among the three fibrosis patterns employed in this study, patchy fibrosis

pattern exhibited the highest MFE. When the fibrosis amount was 40% or less, compact fibrosis pattern exhibited the second-highest MFE. However, at 50% fibrosis, diffuse fibrosis tends to exhibit a higher value of MFE than compact fibrosis. High MFE entropy is associated with ventricular regions featuring a high degree of intermingling between fibrotic and non-fibrotic tissue. Hence, the fibrosis distribution in patchy fibrosis is highly chaotic, whereas diffuse fibrosis is less chaotic.

The arrhythmogenic properties of the fibrosis patterns were analyzed by electrophysiological simulations under reentry induced by the S1-S2 protocol. An S2 stimulation was preceded by three S1 stimulations from the apex of the ventricle. The 3D electrophysiological simulation responses under reentry condition revealed that the CV required to sustain the reentrant wave generated increased consistently as the diffuse fibrosis amount increased from 10% to 50% (Fig. 4A). This correlation between arrhythmogenesis and diffuse fibrosis amount is a result of small fibrosis tissue interspersed among cardiomyocytes throughout the ventricular model. It is highly unlikely that fibrosis is prevalent in a region, and less prevalent or absent in other regions. Therefore, ventricular models that had equal amounts of fibrosis exhibited similar fibrosis textures (Fig. 2). Fig. 3 also shows that diffuse fibrosis exhibited the least MFE among the fibrosis patterns. Consequently, simulations with equal amounts of diffuse fibrosis albeit different distributions exhibited almost similar arrhythmogenic profiles. This observation agrees with the report of Kazbanov et al. [25] that the arrhythmogenesis of diffuse fibrosis depends on both the amount of fibrosis and the spatial distribution of fibrosis.

In contrast, a strong correlation between fibrotic spatial distribution and the arrhythmogenic effect was apparent in electrical simulations under patchy and

compact fibrosis forms. In these forms, the correlation between fibrosis amount and ventricular arrhythmogenesis is non-linear. The higher MFE of patchy and compact fibrosis patterns caused simulations with equal fibrosis amounts to exhibit different arrhythmogenesis. In certain simulations, a marginal amount of patchy fibrosis tended to exhibit higher arrhythmogenic potential than a large amount of patchy fibrosis. This is owing to the non-uniform distribution of fibrosis in the ventricular models, notwithstanding the identical overall fibrosis amount. This effect was more aggravated in compact fibrosis patterns. During reentry, the activation wave anchors and rotates around PS points. We detected PSs during the electrophysiological simulation under fibrosis. We demonstrated that the average PS was higher in the electrophysiological simulations under compact fibrosis than those under patchy and diffuse fibrosis. A lower number of PSs was detected in the electrophysiological simulations under diffuse fibrosis. We also examined the effect of electrical instability induced by fibrosis, on the mechanical performance of the LV. Our results demonstrated that the ventricular models with compact fibrosis distributions yielded a lower average LV-SV, whereas those with diffuse fibrosis yielded a higher average LV-SV. The electrical perturbation predisposed by fibrosis significantly impacted the reduction in the pumping efficacy of the LV.

Our study had several limitations to be addressed. First, the arrhythmogenic propensity of interstitial fibrosis was not considered in our study. Second, the electrical conductivity through tissue was isotropic conductivity. Third, we employed one-way coupling by extracting Ca^{2+} information from electrical activation and furnished it to the mechanical stimulation. The feedback from the mechanical stimulation to the electrical stimulation owing to stretch-activated channels was not considered.

Conclusions

Fibrosis affects the electrophysiological properties of ventricles by diminishing the gap-junction between myocytes. This predisposes conduction delay and conduction block, which are the fundamental preconditions for reentry triggering and perpetuation. Abundant fibrosis tissue in the myocardium is associated with increased arrhythmogenesis. In addition, the spatial distribution of fibrosis also plays a major role in determining arrhythmogenesis. Overall, the likelihood of sustaining reentry in the 3D ventricular model under reentry condition was higher as the volume of fibrosis in the ventricular model increased in all the fibrosis patterns considered in this study. Variation in the spatial distribution of fibrosis substantially affected the arrhythmogenesis of patchy and compact fibrosis than that of diffuse fibrosis. The electrical instability caused by fibrosis was characterized by an average number of PSs. Hence, the average number of PSs detected in electrophysiological simulation under compact fibrosis was higher than those under diffuse and patchy fibrosis. The average number of PSs detected under diffuse fibrosis was lower than those under patchy and compact fibrosis. As a result, the mechanical responses under compact fibrosis significantly reduced the SV of the LV from that under patchy and diffuse fibrosis patterns.

Declarations

Ethics approval and consent to participate

Not applicable

Consent for publication

Not applicable

Availability of data and material

All of the data and material is written in the manuscript and available during request.

Competing interests

Not applicable

Funding

This research was partially supported by basic engineering research project (2016R1D1A1B0101440) and the EDISON Program (NRF-2011-0020576) supervised by NRF.

Author's contributions

This work is the product of intellectual work of the entire team. All the members contributed (to varying degrees) to the analytical methods used, research concept, simulation design, simulation source code, simulation process, and writing of the manuscript.

Simulation, Data analysis, Writing – original draft: Abrha Abebe Tekle

Methodology design, Writing – review & editing: Ki Moo Lim

Acknowledgements

Not applicable

References

1. Rossi MA: Connective tissue skeleton in the normal left ventricle and in hypertensive left ventricular hypertrophy and chronic chagasic myocarditis. *Med Sci Monit* 2001, 7(4):820-832.
2. Jugdutt BI: Remodeling of the myocardium and potential targets in the collagen degradation and synthesis pathways. *Current Drug Targets-Cardiovascular & Hematological Disorders* 2003, 3(1):1-30.
3. de Bakker JM, Stein M, van Rijen HV: Three-dimensional anatomic structure as substrate for ventricular tachycardia/ventricular fibrillation. *Heart Rhythm* 2005, 2(7):777-779.
4. de Bakker JM, van Rijen HM: Continuous and discontinuous propagation in heart muscle. *Journal of cardiovascular electrophysiology* 2006, 17(5):567-573.
5. Kawara T, Derksen R, de Groot JR, Coronel R, Tasseron S, Linnenbank AC, Hauer RN, Kirkels H, Janse MJ, de Bakker JM: Activation delay after premature stimulation in chronically diseased human myocardium relates to the architecture of interstitial fibrosis. *Circulation* 2001, 104(25):3069-3075.
6. Burt JR, Zimmerman SL, Kamel IR, Halushka M, Bluemke DA: Myocardial T1 mapping: techniques and potential applications. *Radiographics* 2014, 34(2):377-395.
7. Everett IV TH, Olgin JE: Atrial fibrosis and the mechanisms of atrial fibrillation. *Heart Rhythm* 2007, 4(3):S24-S27.
8. Nakai T, Chandy J, Nakai K, Bellows WH, Flachsbart K, Lee RJ, Leung JM: Histologic assessment of right atrial appendage myocardium in patients with atrial fibrillation after coronary artery bypass graft surgery. *Cardiology* 2007, 108(2):90-96.
9. Strain JE, Grose RM, Factor S, Fisher JD: Results of endomyocardial biopsy in patients with spontaneous ventricular tachycardia but without apparent structural heart disease. *Circulation* 1983, 68(6):1171-1181.
10. Assomull RG, Prasad SK, Lyne J, Smith G, Burman ED, Khan M, Sheppard MN, Poole-Wilson PA, Pennell DJ: Cardiovascular magnetic resonance, fibrosis, and prognosis in dilated cardiomyopathy. *Journal of the American College of Cardiology* 2006, 48(10):1977-1985.
11. John BT, Tamarappoo BK, Titus JL, Edwards WD, Shen W-K, Chugh SS: Global remodeling of the ventricular interstitium in idiopathic myocardial fibrosis and sudden cardiac death. *Heart Rhythm* 2004, 1(2):141-149.
12. Gardner P, Ursell P, Fenoglio Jr J, Wit A: Electrophysiologic and anatomic basis for fractionated electrograms recorded from healed myocardial infarcts. *Circulation* 1985, 72(3):596-611.
13. De Bakker J, Van Capelle F, Janse MJ, Tasseron S, Vermeulen JT, De Jonge N, Lahpor JR: Slow conduction in the infarcted human heart.'Zigzag'course of activation. *Circulation* 1993, 88(3):915-926.
14. Rushton WAH: Initiation of the propagated disturbance. *Proceedings of the Royal Society of London Series B-Biological Sciences* 1937, 124(835):210-243.
15. Fozzard H, Schoenberg M: Strength—duration curves in cardiac Purkinje fibres: effects of liminal length and charge distribution. *The Journal of physiology* 1972, 226(3):593-618.

16. Tanaka K, Zlochiver S, Vikstrom KL, Yamazaki M, Moreno J, Klos M, Zaitsev AV, Vaidyanathan R, Auerbach DS, Landas S: Spatial distribution of fibrosis governs fibrillation wave dynamics in the posterior left atrium during heart failure. *Circulation research* 2007, 101(8):839-847.
17. De Jong S, van Veen TA, van Rijen HV, de Bakker JM: Fibrosis and cardiac arrhythmias. *Journal of cardiovascular pharmacology* 2011, 57(6):630-638.
18. Pertsov A: Scale of geometric structures responsible for discontinuous propagation in myocardial tissue. *Discontinuous Conduction in the Heart* 1997:273-293.
19. Turner I, L.-H. HUANG C, Saumarez RC: Numerical simulation of paced electrogram fractionation: relating clinical observations to changes in fibrosis and action potential duration. *Journal of cardiovascular electrophysiology* 2005, 16(2):151-161.
20. Panfilov A: Spiral breakup in an array of coupled cells: the role of the intercellular conductance. *Physical review letters* 2002, 88(11):118101.
21. Ten Tusscher K, Panfilov A: Influence of nonexcitable cells on spiral breakup in two-dimensional and three-dimensional excitable media. *Physical Review E* 2003, 68(6):062902.
22. ten Tusscher KH, Panfilov AV: Wave propagation in excitable media with randomly distributed obstacles. *Multiscale Modeling & Simulation* 2005, 3(2):265-282.
23. Spach MS, Heidlage JF, Dolber PC, Barr RC: Mechanism of origin of conduction disturbances in aging human atrial bundles: experimental and model study. *Heart rhythm* 2007, 4(2):175-185.
24. Kuijpers N, Keldermann R, Arts T, Hilbers P: Computer simulations of successful defibrillation in decoupled and non-uniform cardiac tissue. *EP Europace* 2005, 7(s2):S166-S177.
25. Kazbanov IV, Ten Tusscher KH, Panfilov AV: Effects of heterogeneous diffuse fibrosis on arrhythmia dynamics and mechanism. *Scientific reports* 2016, 6:20835.
26. Ten Tusscher K, Panfilov A: Cell model for efficient simulation of wave propagation in human ventricular tissue under normal and pathological conditions. *Physics in medicine and biology* 2006, 51(23):6141.
27. Corradi D, Callegari S, Maestri R, Benussi S, Alfieri O: Structural remodeling in atrial fibrillation. *Nature Reviews Cardiology* 2008, 5(12):782.
28. Nattel S, Burstein B, Dobrev D: Atrial remodeling and atrial fibrillation: mechanisms and implications. *Circulation: Arrhythmia and Electrophysiology* 2008, 1(1):62-73.
29. Li D, Fareh S, Leung TK, Nattel S: Promotion of atrial fibrillation by heart failure in dogs: atrial remodeling of a different sort. *Circulation* 1999, 100(1):87-95.
30. Burstein B, Comtois P, Michael G, Nishida K, Villeneuve L, Yeh Y-H, Nattel S: Changes in connexin expression and the atrial fibrillation substrate in congestive heart failure. *Circulation research* 2009, 105(12):1213-1222.
31. Rice JJ, Wang F, Bers DM, De Tombe PPJBj: Approximate model of cooperative activation and crossbridge cycling in cardiac muscle using ordinary differential equations. 2008, 95(5):2368-2390.

32. Guccione JM, Costa KD, McCulloch ADJJob: Finite element stress analysis of left ventricular mechanics in the beating dog heart. 1995, 28(10):1167-1177.
33. Usyk TP, LeGrice IJ, McCulloch ADJC, science vi: Computational model of three-dimensional cardiac electromechanics. 2002, 4(4):249-257.
34. Gurev V, Constantino J, Rice J, Trayanova NJBj: Distribution of electromechanical delay in the heart: insights from a three-dimensional electromechanical model. 2010, 99(3):745-754.
35. Zahid S, Cochet H, Boyle PM, Schwarz EL, Whyte KN, Vigmond EJ, Dubois R, Hocini M, Haissaguerre M, Jais P, Trayanova NA: Patient-derived models link re-entrant driver localization in atrial fibrillation to fibrosis spatial pattern. *Cardiovasc Res* 2016, 110(3):443-454.
36. Iyer AN, Gray RA: An experimentalist's approach to accurate localization of phase singularities during reentry. *Annals of biomedical engineering* 2001, 29(1):47-59.
37. Marrouche NF, Wilber D, Hindricks G, Jais P, Akoum N, Marchlinski F, Kholmovski E, Burgon N, Hu N, Mont L: Association of atrial tissue fibrosis identified by delayed enhancement MRI and atrial fibrillation catheter ablation: the DECAAF study. *Jama* 2014, 311(5):498-506.
38. Nguyen TP, Qu Z, Weiss JN: Cardiac fibrosis and arrhythmogenesis: the road to repair is paved with perils. *Journal of molecular and cellular cardiology* 2014, 70:83-91.

Figures

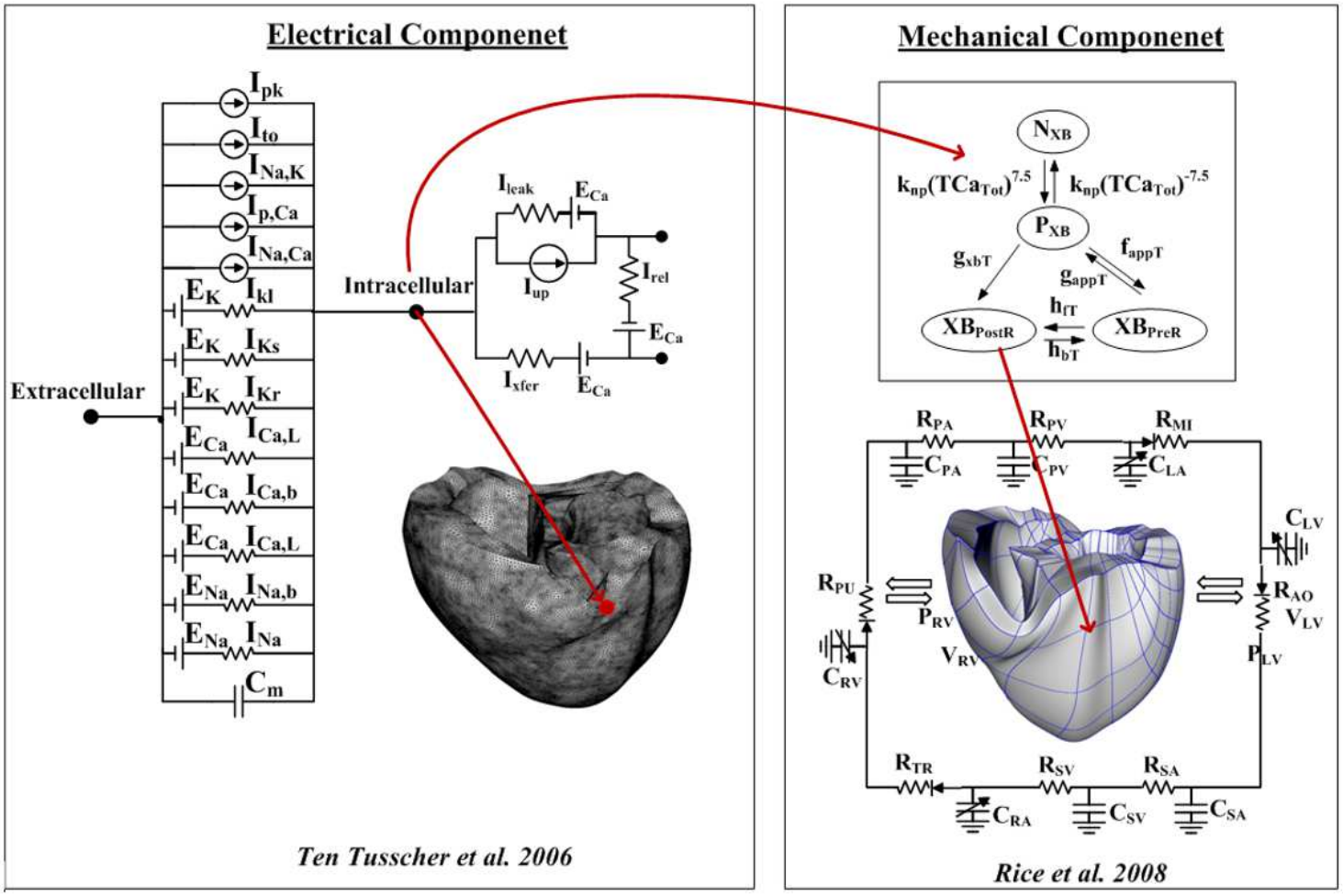

Figure 1

Schematic of excitation–contraction coupling model of a human ventricular cell adapted from previous studies (Heikhmakhtiar et al., 2018a;Heikhmakhtiar et al., 2018b;Dusturia et al., 2019). The left side of the diagram is an electrical model that depicts a human ventricular cell model that simulates the ion exchange process through the cell membrane. The electrical model is the Ten Tusscher human ventricular cell model. The mechanical component on the right is the myofilament models developed by Rice et al.

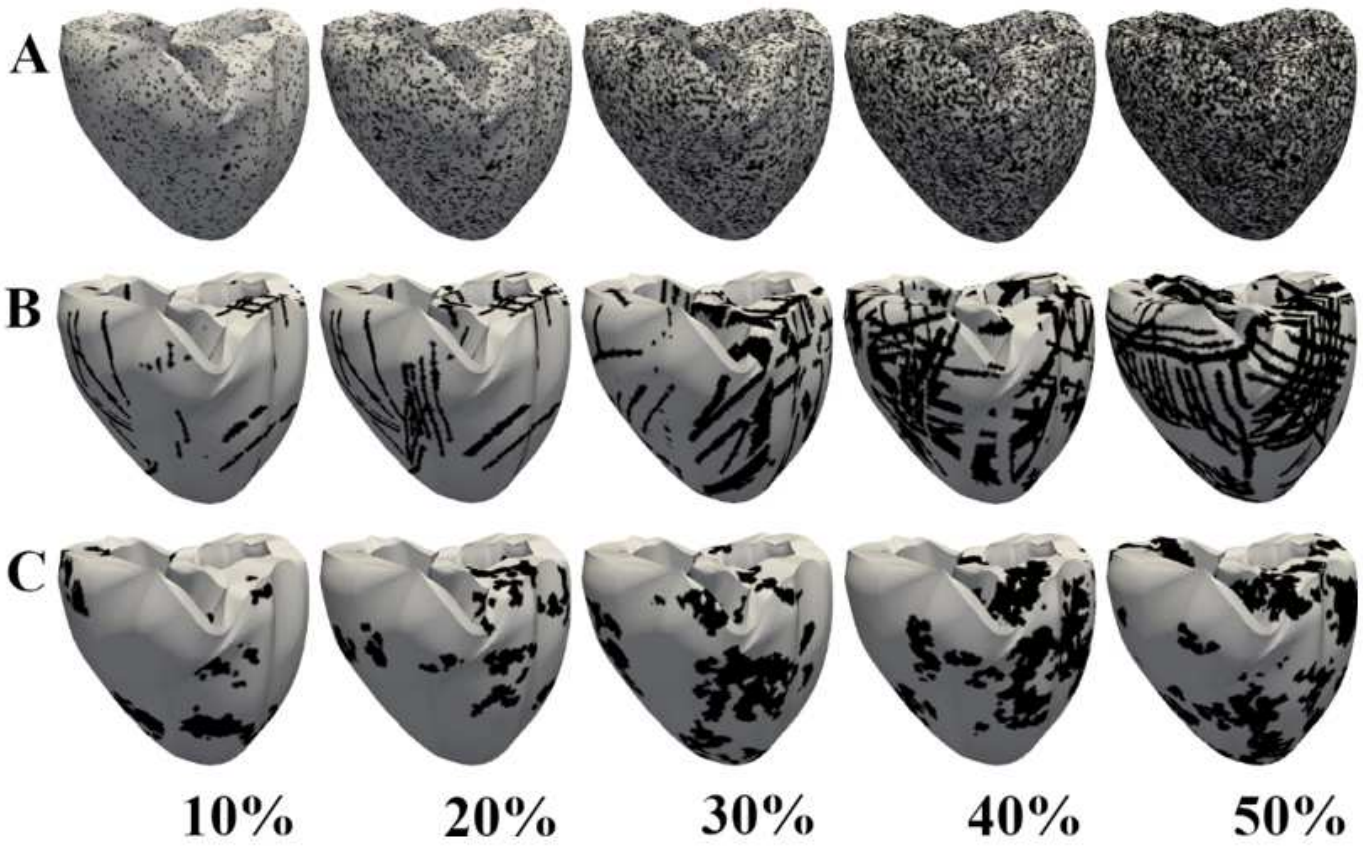

Figure 3

Fibrosis patterns generated. Diffuse (A), patchy (B), and compact (C) fibrosis patterns. The black regions indicate areas of fibrosis.

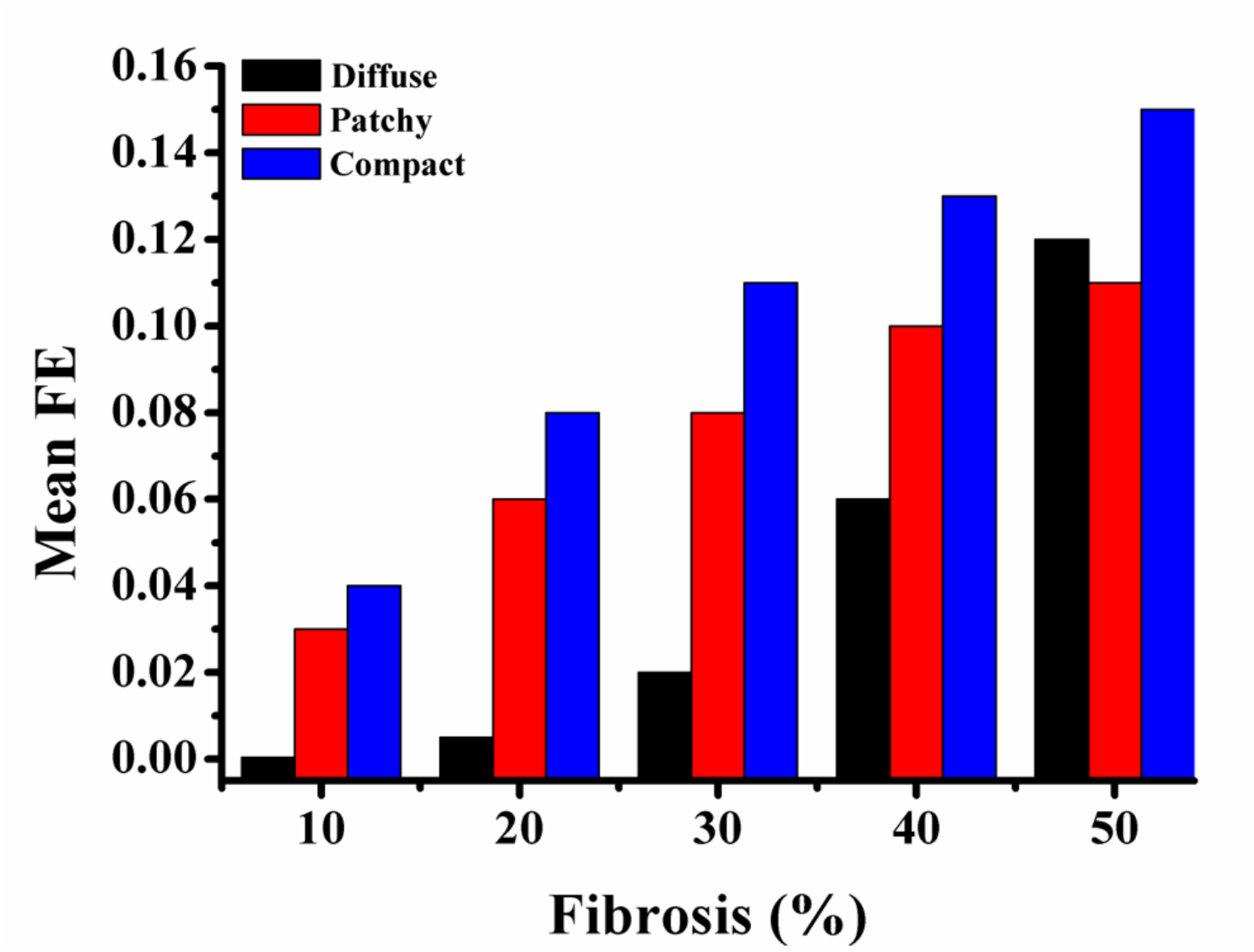

Figure 5

Mean fibrosis entropy of diffuse, compact, and patchy fibrosis.

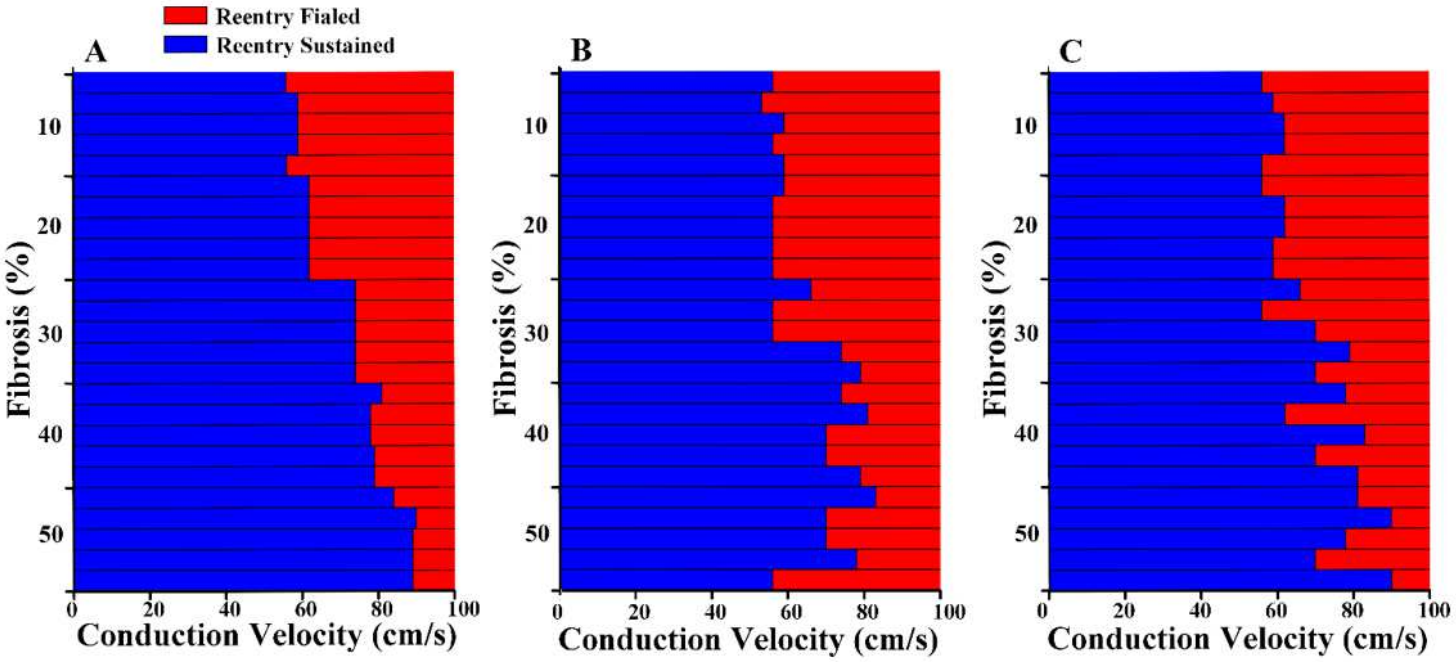

Figure 7

Conduction delay owing to fibrosis distribution and fibrosis amount of (A) diffuse fibrosis, (B) patchy fibrosis, and (C) compact fibrosis.

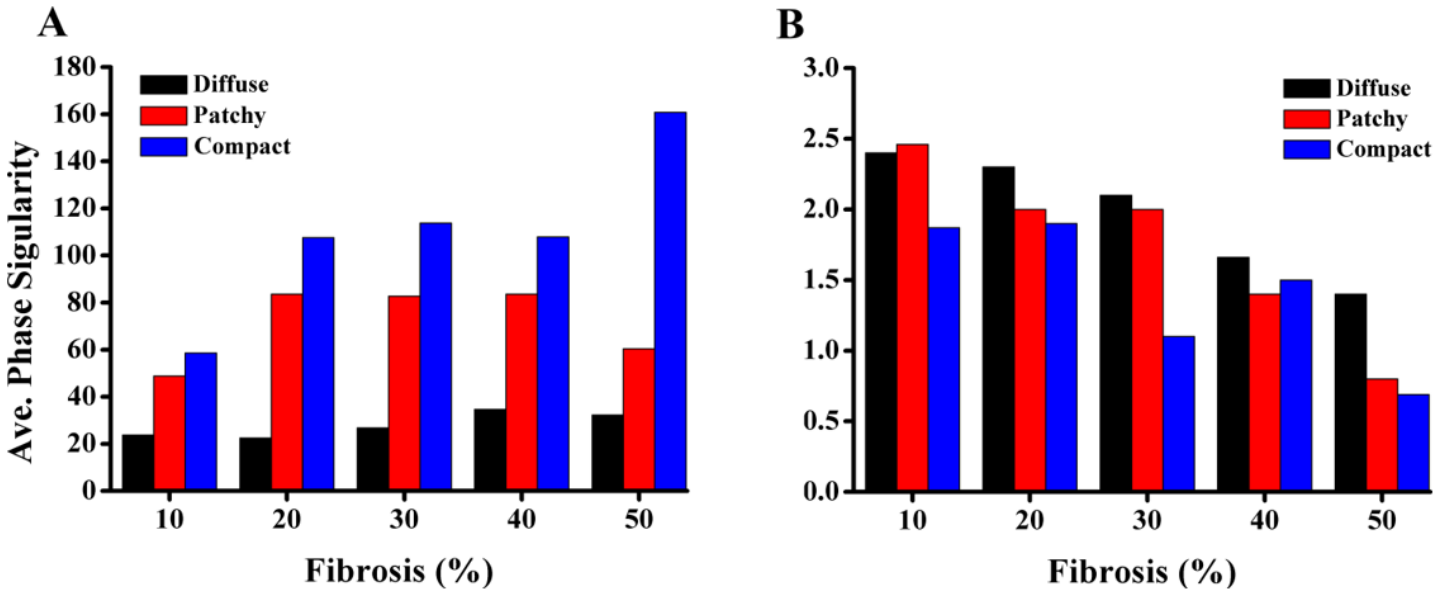

Figure 9

Electrical and mechanical influence of fibrosis types and fibrosis amount. (A) Average number of phase singularities and (B) average left-ventricle stroke volume.